Open Archive TOULOUSE Archive Ouverte (OATAO)

A device to achieve low Reynolds numbers in an open surface water channel

Alexander Radi · David Lo Jacono ·
John Sheridan

Abstract When investigating flow structures, and especially flow transitions, research projects often seek to increase insight using complementary numerical and physical experiments. Obtaining exact Reynolds number correspondence can frequently be difficult in experiments, particularly when relatively low values are required. Often, available test facilities were designed and optimised for a specific velocity range, meaning they have restrictions on the minimum flow velocity. This study describes a device to reduce the flow velocity locally in an open surface water channel. The underlying idea is to divert a controlled fraction of the incoming flow from the working section by increasing the pressure there, resulting in reduced velocity. This idea is realised using a 'sub-channel' that can be inserted into the main test chamber, with a variable porosity perforated screen at its downstream end. This study assesses and optimises the flow quality inside this structure, such as usable test section length, uniformity of the velocity profiles and turbulence intensity. The results demonstrate that the device creates high quality low

Reynolds number flows, which is exemplified with the canonical circular cylinder in cross-flow.

1 Introduction

The open surface water channel at Fluids Laboratory for Aeronautical and Industrial Research (FLAIR) at Monash University has been used successfully for over 10 years in research on the flow over bluff bodies. Its velocity range is 0.045–0.5 m/s, with a flow quality comparable to other world class facilities, as has been shown in a variety of experiments (Carberry et al. 2005; Nazarinia et al. 2009; Nemes et al. 2012).

Commonly, these experiments are accompanied by a numerical study (Ryan et al. 2007; Leontini et al. 2011; Leontini and Thompson 2012). However, attaining correspondence between the numerical and experimental results is often difficult because of the different Reynolds numbers achievable in computations (usually low) and experiments (usually high). This correspondence can be improved by extending the Reynolds number range of an existing water channel facility.

Three parameters determine the minimum Reynolds number $Re = dU/v$: the fluid viscosity v, model dimension d and the freestream velocity U. The minimum model dimension d is often prescribed by experimental requirements, such as model stiffness, manufacturing process or minimum spatial resolution of particle image velocimetry (PIV) recordings.

The kinematic viscosity v can be adjusted by changing the fluid temperature or using a different working fluid altogether. The high viscosity of e.g. mineral oil is often exploited in insect flight or micro-air vehicles research (Bechert et al. 1992; Wang et al. 2004; Willert

A. Radi (✉) · D. Lo Jacono · J. Sheridan
FLAIR, Department of Mechanical and Aerospace Engineering,
Monash University, Melbourne, VIC 3800, Australia
e-mail: Alexander.Radi@monash.edu

J. Sheridan
e-mail: john.sheridan@monash.edu

D. Lo Jacono
INPT, UPS, IMFT (Institut de Mécanique des Fluides de
Toulouse), Université de Toulouse, Allée Camille Soula,
31400 Toulouse, France

D. Lo Jacono
CNRS, IMFT, 31400 Toulouse, France

et al. 2010). A more exotic way of modifying the (effective) viscosity is to use a 'flowing soap film', where the viscosity is also a function of the film thickness (Vorobieff and Ecke 1999).

The last parameter, the freestream velocity U, is limited solely by the specifications of the research facility. But reducing the velocity of an existing recirculating water channel has its limitations. Tunnels are designed for a certain velocity range, with the turbulence management system optimised for that range. Decreasing the channel speed far below specifications can affect the turbulence level and frequency content of the flow and—more importantly—can have a negative effect on the uniformity of the flow, leading to skewed velocity profiles in the test chamber.

To avoid these adverse effects, it is proposed to modify the flow velocity only locally, by splitting the flow inside the main channel test chamber. A U shaped sub-channel insert, with a perforated screen at its downstream end, was built (Fig. 1). The screen creates a pressure drop, which leads to a pressure increase within this structure. The remaining flow bypasses it at higher velocity, keeping the overall flow rate through the water channel unchanged. The porosity of the screen α, defined as the ratio of the open area A_{open} to the total area of the screen A_{total}, determines the degree of velocity reduction.

The flow uniformity and turbulence intensity inside this device are the primary concern of this study. The design and construction of the sub-channel are described in Sect. 2, followed by an investigation of flow uniformity and turbulence intensity in Sect. 3. The performance of the device in an experiment is demonstrated in Sect. 4 on the canonical case of a circular cylinder in cross-flow.

2 Experimental set-up

2.1 Main structure

The test section of the FLAIR water channel has a width of 600 mm, with a water depth $h = 760$ mm. The sub-channel (Fig. 1) is designed to occupy two-thirds of this cross-section area. Its (inner) width is $W = 360$ mm, leaving 110 mm on each side to the main channel walls for the bypass flow. The side walls ($L \times H = 1{,}020 \times 855$ mm) and bottom plate of the insert are made of 10-mm thick transparent acrylic. The leading edges of the side walls and the bottom plate are elliptical, with a main-axis ratio of 4:1. The experimental model can be attached to the bottom plate, approximately $L/3$ downstream of the leading edges ($x = 335$ mm). The rear screen consists of two perforated acrylic sheets, with adjustable porosity α.
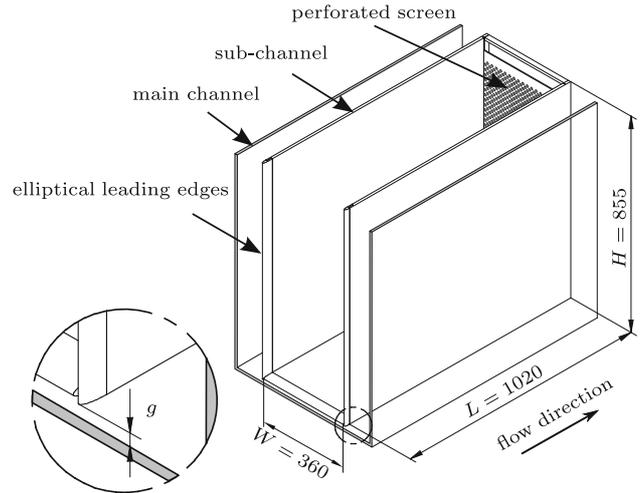

Fig. 1 Geometry of the sub-channel insert placed in the main channel test section. Note the gap size g
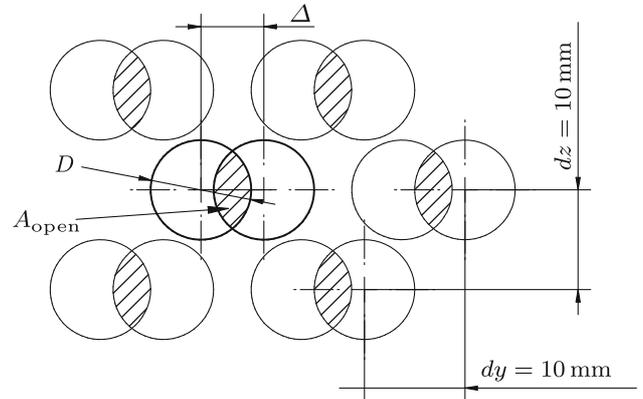

Fig. 2 Holes pattern of the perforated screen, when the two acrylic sheets are shifted with respect to each other by the distance Δ. The open area of the screen is *dashed*

The sub-channel can be suspended in the channel test chamber, leaving a gap of size g between its bottom plate and the main channel floor, or placed directly onto the floor. In Sect. 3.2.3, it will be shown that this gap width has to be chosen carefully to achieve uniform velocity profiles inside the sub-channel.

2.2 Perforated screen

The adjustable screen consists of two perforated acrylic sheets of 3 mm thickness. A staggered pattern of over 1,200 holes of diameter $D = 10$ mm was drilled into each sheet. By overlaying the two sheets and shifting them horizontally with respect to each other as shown in Fig. 2, the ratio of open area A_{open} to total screen area A_{total} can be varied continuously. For a fully open screen (shift distance

$\Delta = 0$), the porosity is $\alpha = \pi/8 \approx 0.393$. When decreasing the open area, this ratio varies according to Eq. 1.

$$\alpha = \frac{A_{\text{open}}}{A_{\text{total}}} = 0.393 \left(\frac{2\arccos(\delta)}{\pi} - \frac{2\delta}{\pi}\sqrt{1-\delta^2} \right)$$
$$\text{where } \delta = \frac{\Delta}{D} \tag{1}$$

Seven values of α, between 0.393 and 0.0041, were chosen for the tests. Alignment holes were drilled into both acrylic sheets in such a way that these values could be reproduced accurately by the insertion of a metal pin.

The screen can be removed easily, by sliding it vertically along grooves machined in the side walls. This allows quick adjustment of α between experiments, without requiring the complete structure being removed from the water channel.

2.3 Instrumentation

The two-component laser doppler velocimetry system (LDV) consisted of an argon-ion laser, a 'Colourburst' multicolour beam generator and a TR260 fiberoptic probe by TSI®. The probe was aligned perpendicular to the channel glass walls and moved by an Isel® three-axis traverse. Due to the focal length of the probe's lens, only half of the tunnel width could be sampled.

PIV data were recorded with a PCO®2000 camera in double-shutter mode, fitted with a 50 mm lens. A pulsed Nd:YAG laser created a 3-mm thick light sheet. It was directed up through the tunnel glass bottom and aligned parallel to the flow direction. The cross-correlation was performed with an in-house code (Fouras et al. 2008) using an interrogation window size of 32×32 pixels with 50 % overlap.

The Strouhal numbers of the circular cylinder wake (carbon fibre cylinder, $d = 6$ mm) were measured with a hot film probe, operated in constant temperature mode. The probe was placed at $(x, y) \approx (5d, -1.5d)$, with the wire aligned parallel to the cylinder main axis. The analogue signal was low-pass filtered at 10 Hz and sampled at 20 Hz. At each Reynolds number, a velocity time series of 20 min was recorded (equivalent to 440–600 main shedding cycles). The Reynolds numbers were increased stepwise from 100 to 300; then the series was reversed, to capture any hysteretic effects in the flow. The water temperature was measured throughout the experiments to correct for changes in viscosity. The freestream velocity was recorded simultaneously with LDV upstream of the model.

The uncertainties of the Reynolds and Strouhal numbers were ± 1.6 and ± 1.5 %, respectively, at a confidence interval of 95 % (at $Re = 200$). The precision limit of the LDV freestream velocity measurement was ± 0.14 %.
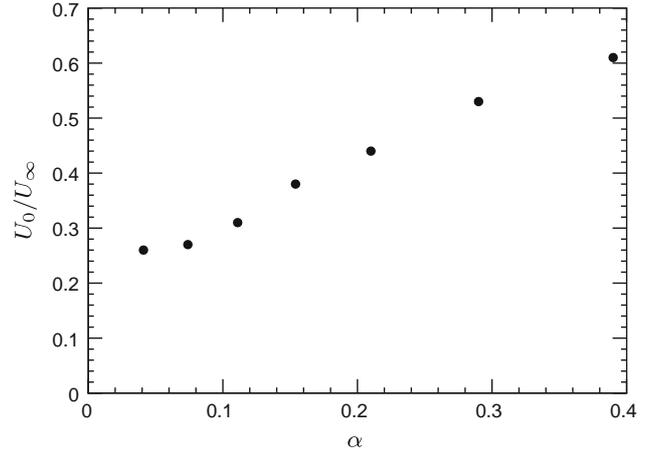

Fig. 3 Freestream velocity reduction inside the sub-channel as a function of screen porosity α, measured at model location ($x = L/3$, $y = 0$, $z = h/2$) and $U_\infty = 0.09$ m/s. *Error bars are smaller than the symbols*

3 Validation

The coordinates refer to a right-hand coordinate system, whose origin is in the centre plane at the bottom leading edge of the sub-channel, with x and z pointing in streamwise and vertical directions, respectively. u, v and w are the streamwise, spanwise and vertical velocity components. A velocity time series $u(t)$ is decomposed into $u(t) = U + u'(t)$, where U is the time-averaged and $u'(t)$ is the fluctuating component. The velocity in the empty main channel test section (sub-channel not inserted) is referred to as U_∞. Cross-sectional velocities are presented as a relative local difference $U_{\text{diff}} = (U - <U>)/<U>$ to the average velocity of the whole crosssection $<U>$. The average flow velocity at model location ($x \approx L/3$) is referred to as U_0. The turbulence intensity estimates from LDV measurements are based on root-mean-squares of two velocity components:

$$Tu = \frac{\sqrt{\frac{1}{2}\left(\overline{u'^2} + \overline{w'^2}\right)}}{<U>} \tag{2}$$

The tested velocity range in this study was $0.045 \leqslant U_\infty \leqslant 0.135$ m/s.

3.1 Velocity reduction capability

The dependence of freestream velocity inside the sub-channel at model location on porosity α is shown in Fig. 3. The main channel flow velocity can be reduced to 60–30 %, depending on α.

Figure 4 shows the development of the streamwise velocity along the channel centreline (at $z/h \approx 0.5$) for two channel pump settings and two values of α. Velocity reduction can be seen to have occurred already upstream of
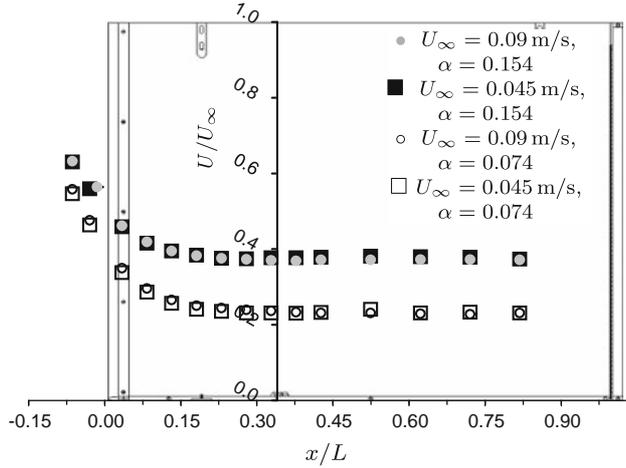
Fig. 4 Development of streamwise velocity inside the sub-channel along the centreline. Data for two pump speeds and two values of α are overlaid on a side view of the sub-channel. *Error bars* are smaller than the symbols. The flow is from *left to right*

the sub-channel entrance. The flow slows down monotonically as it enters the structure and reaches a constant velocity latest at one third into the sub-channel. For $x > L/3$, the velocity variations stay below ± 2 % (relative to the velocity average at $x > L/3$).

3.2 Flow quality

3.2.1 Comparison to the main channel flow

The flow uniformity and turbulence intensity of the sub-channel crosssection at model location were compared with the base case of the empty main channel test chamber. The LDV point velocity measurements were taken in a plane perpendicular to the flow direction. The focal length of the LDV lens allowed to traverse only half of the channel width; flow symmetry will be assumed. Between 4 and 6 min were recorded per sampling point.

Figure 5 shows the streamwise velocity contour maps, overlaid with turbulence intensity contour lines (turbulence contour levels: 1, 1.5, 2, 3, 4, 6, 8 %). The vertical direction is measured from the sub-channel bottom plate and is non-dimensionalised by the water depth h.

It can be seen that at the higher flow velocity, the sub-channel velocity variations remain largely within ± 1 % of the plane average, with a mild velocity gradient along the vertical direction in the centre plane. The turbulence intensity lies between 1.5 and 2 %, which is comparable to the empty test section.

The origin of the velocity deficit and increased turbulence intensity in the bottom corner of the main channel crosssection (Fig. 5a, c) is not clear, but this defect is not reproduced in the sub-channel.
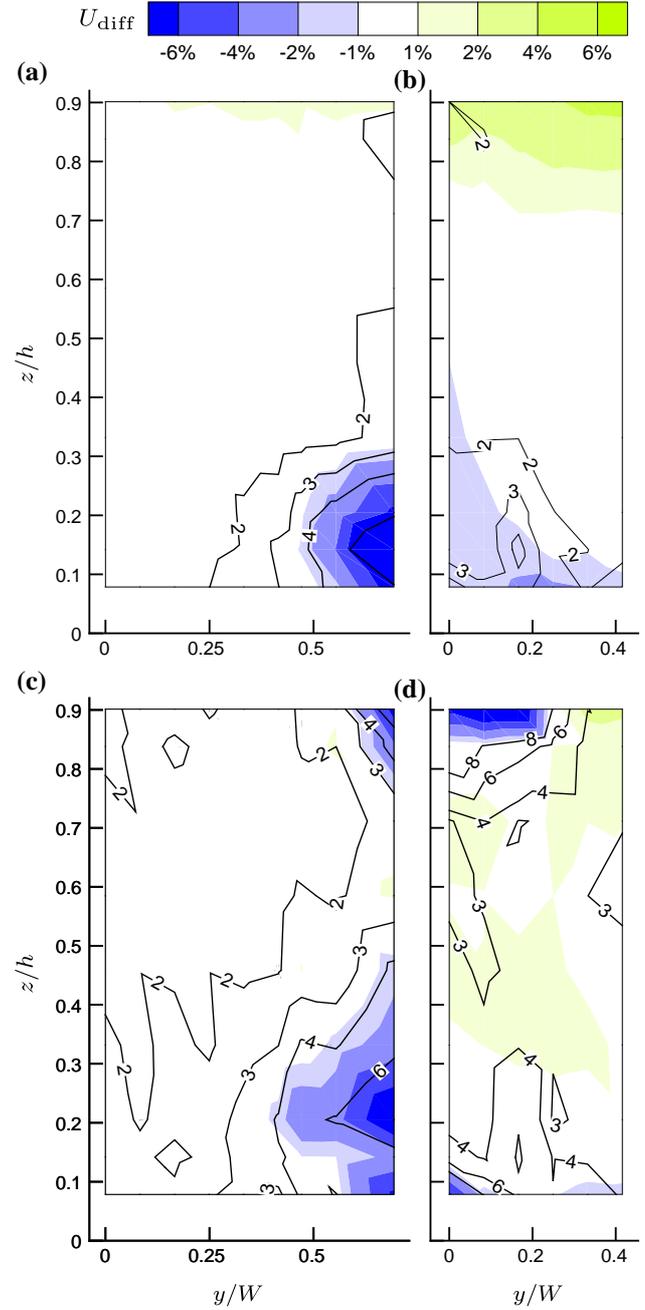

Fig. 5 Comparison of flow uniformity in the empty test section (*left side*) with the flow in the sub-channel at model location (*right side*) at two freestream velocities: **a, b** $U_\infty = 0.045$ m/s, **c, d** $U_\infty = 0.135$ m/s. The *colour contours* show U_{diff}; the *contour lines* represent Tu[%]. ($\alpha = 0.154$, $g = 5$ mm)

Further tests indicated that for freestream velocities above the ones investigated in Fig. 5, and for screen porosities larger than $\alpha = 0.154$, the flow quality in the sub-channel is comparable to the empty test section. For lower velocities and/or lower porosities, the flow quality deteriorated rapidly. This will be discussed in Sect. 3.2.4.
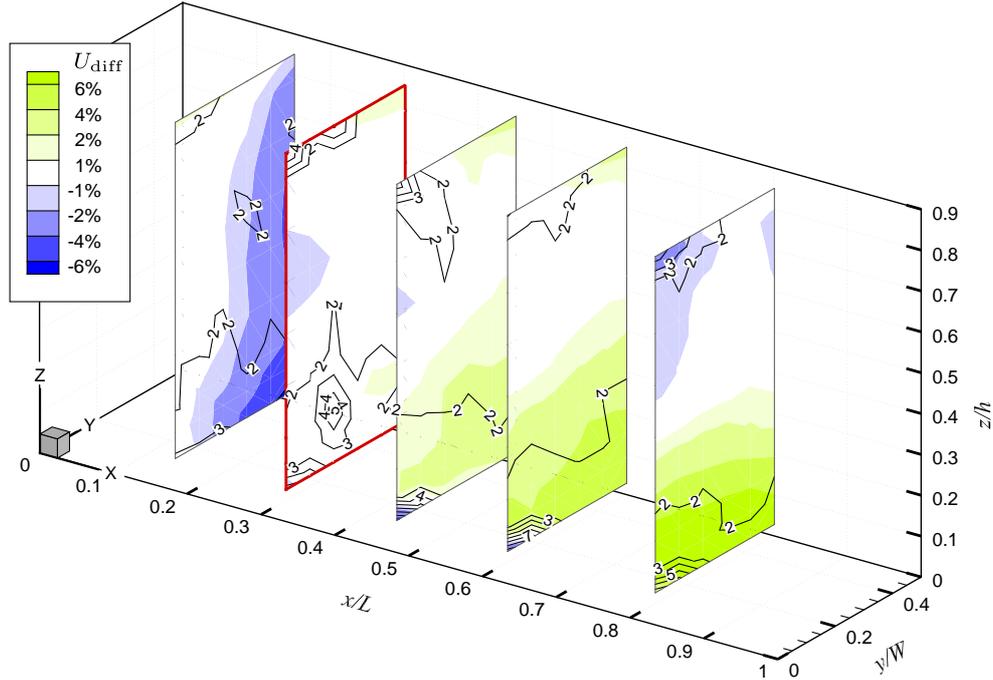
Fig. 6 Steamwise velocity and turbulence contours in five half-planes of the sub-channel (the coordinate origin is in the symmetry plane). The *colour contours* show U_{diff}; the *contour lines* represent Tu [%].

The plane at model location is marked by the *bold red frame*. ($U_\infty = 0.90\,\text{m/s}$, $\alpha = 0.154$, $g = 5\,\text{mm}$)

3.2.2 Dependence on the streamwise location

To study the flow quality throughout the streamwise extent of the sub-channel, LDV measurements in 5 cross-stream half-planes 150 mm apart were taken. The streamwise velocity in all planes of Fig. 6 is non-dimensionalised by the average velocity of the plane at model location (marked by the bold red frame).

The data show that the turbulence intensity remains largely between 1.5 and 2 % throughout the sub-channel, which is equivalent to the empty test section. Upstream of the model location, a horizontal velocity gradient is visible, with velocities close to the side wall being up to 6 % lower. This is a remnant of the flow expansion at the sub-channel entrance. This horizontal gradient vanishes at model location. Downstream of the model location, a vertical velocity gradient develops, with the flow in the bottom third of the sub-channel being up to 6 % faster than the average. The upper two-thirds of the flow field maintain a constant velocity (within ± 2 %) throughout the sub-channel extent. These data suggest that the suitable range for experimental measurements spans $x > L/3$, $z > h/3$ and all of y/W.

3.2.3 Dependence on the gap size g

A particularly interesting effect was observed during preliminary experiments: The first version of the sub-channel did not possess a bottom plate, but was standing on the water channel floor. Representing an obstacle to the incoming floor boundary layer, the whole structure induced a standing vortex ('horse-shoe vortex') of 15–20 cm in diameter at its entrance. The vortex collapsed periodically, and its remains were advected through the sub-channel, which led to unacceptably large velocity fluctuations inside the structure.

To suppress this phenomenon, the sub-channel was suspended in the main test chamber, with its bottom plate above the floor boundary layer. A study was undertaken to determine the effect of the gap size g between the bottom plate and the channel floor (see Fig. 1). It was found that 'large' gap sizes (38, 76 and 114 mm) suppressed the standing vortex, but with the adverse effect of strongly skewed vertical U-velocity profiles inside the sub-channel. Particularly, a velocity deficit of up to 10 % of the profile mean was noticed in the bottom third of the profile, which persisted throughout the streamwise extent of the structure. 'Small' gaps of 2, 5 and 10 mm, on the other hand, achieved the desired effect of suppressing the standing vortex, at the same time leading to uniform velocity profiles.

The increased skewness resulting from large gap sizes can be understood by studying the time-averaged PIV data in Fig. 7. A small gap below the sub-channel—in the order of 5 mm—is sufficient to prevent large-scale boundary
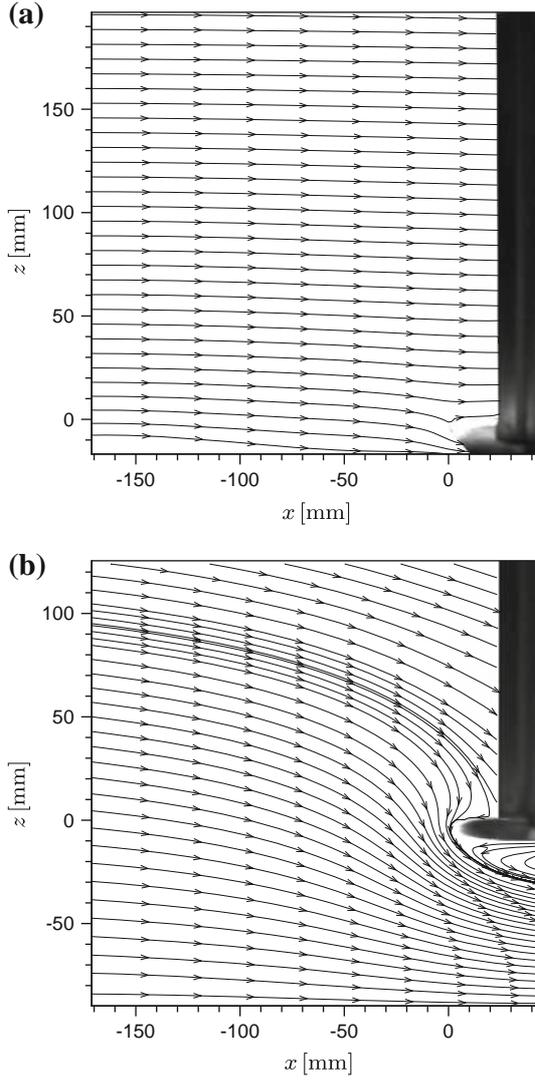
Fig. 7 Time-averaged flow field at the bottom leading edge of the sub-channel, showing the impact of different gap sizes on the flow in the centre plane $y/W = 0$: **a** gap: 5 mm, **b** 76 mm. ($U_\infty = 0.075$ m/s, $\alpha = 0.154$)

Fig. 8 Flow uniformity at model location for three different screen porosities α: **a** 0.041, **b** 0.154, **c** 0.39. The *colour contours* show U_{diff}; the *contour lines* represent *Tu* [%]. The *dots mark* LDV sampling points. ($U_\infty = 0.090$ m/s, $g = 5$ mm)

layer separation upstream of the entrance and a possible build-up of the horse-shoe vortex. In this case, the inflow into the sub-channel is parallel to the bottom plate (Fig. 7a). A large gap, on the other hand, modifies the global inflow by deflecting a large portion of the incoming stream downward into the gap (Fig. 7b). This vertical velocity component requires a reduction in the streamwise component inside the sub-channel to satisfy incompressibility. This streamwise velocity deficit is larger near the bottom plate, which explains the skewed velocity profiles.

Obviously, a compromise has to be found which minimises profile skewness, while preventing the standing vortex. PIV measurements showed that the incoming main channel floor boundary layer thickness was 30–40 mm for the investigated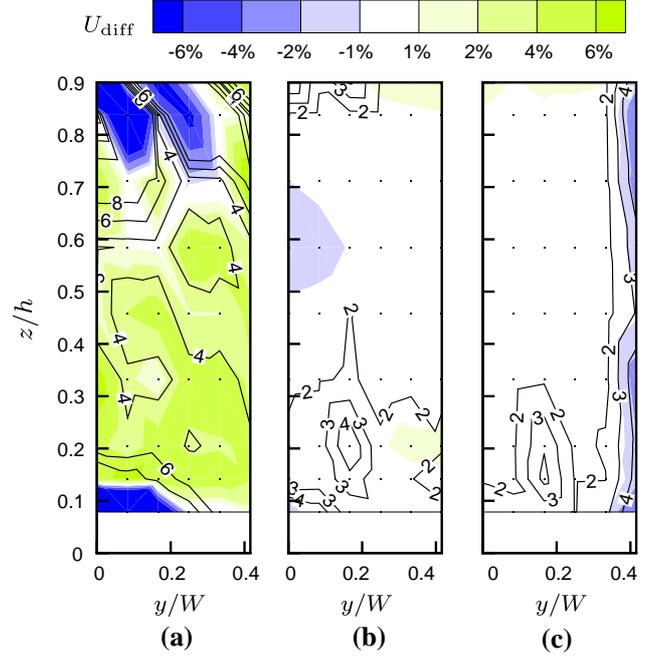 velocities. Assuming a Blasius profile as an approximation for this boundary layer, the displacement thickness is approximately one third of these values, which is just above the range of the 'small' gap sizes investigated. This observation suggests that the gap size should be chosen to be approximately the displacement thickness of the incoming floor boundary layer.

3.2.4 Dependence on the screen porosity α

The flow uniformity at model location was measured for $\alpha = 0.041$, 0.154 and 0.39 at $U_\infty = 0.090$ m/s (Fig. 8). These data suggest that the flow quality does not change considerably for porosities above the medium value $\alpha = 0.154$. The lowest value of α, on the other hand, leads to a deterioration of the flow uniformity inside the sub-channel, as seen in Fig. 8a. The main reason for the bad performance is flow separation on the bottom plate and beneath the water surface at the sub-channel entrance. The separated regions cause the velocity deficits and the high turbulence intensities seen at the top and the bottom of in Fig. 8a.

The limited number of experiments does not provide an explicit α value dividing acceptable and deteriorated flow qualities. But the data from Fig. 8, the results from Sect. 4.1 and our hitherto experiences with the sub-channel show that choosing $\alpha > 0.15$ assures an adequate flow quality for experiments. This conclusion is also supported by Fig. 3, which shows a linear dependence of U_0/U_∞

with screen porosity α within the recommended range of α values. For $\alpha \lesssim 0.1$, the flow behaviour inside the sub-channel changes, such that this linear dependence vanishes.

3.3 Turbulence frequency content

The turbulence spectrum inside the sub-channel was investigated, and no substantial differences to the empty test chamber characteristics were found. The power spectral density of the streamwise velocity inside the sub-channel showed no new dominant peaks compared with the main channel test section.

4 Results and conclusions

4.1 Strouhal numbers of a circular cylinder

The canonical case of a circular cylinder in cross-flow was chosen to evaluate the performance of the sub-channel experimentally. A carbon fibre cylinder was mounted vertically in the sub-channel at $x = L/3$ ($\alpha = 0.154$). Suction tubes, as used by Miller and Williamson (1994), were installed at the cylinder ends 100 diameters apart to induce parallel shedding. The shedding frequency of the von Kármán vortex street was measured in the near-wake by a hot film, as described in Sect. 2.3.

Figure 9 shows the recorded Strouhal number curve as a function of Reynolds number. For $Re < 170$, the Strouhal numbers follow closely the data of Williamson (1992). A discontinuous drop occurs at $Re \approx 177$, which marks the transition from a laminar two-dimensional to a three-dimensional wake and the appearance of mode A (see Williamson 1996b). The Strouhal numbers exhibit a steep, but continuous, increase for Reynolds numbers $225 < Re < 250$, which marks the gradual transfer of disturbance energy from mode A to the second three-dimensional mode B. For $Re > 250$, mode B dominates the wake, and the Strouhal number curve flattens. When decreasing the Reynolds number again, the pronounced hysteresis of the first discontinuity can be seen by a delayed increase in St at $Re \approx 167$.

For the Reynolds number range investigated, our data exhibit all the significant phenomena referred to as the 'natural' transition scenario (Williamson 1996b). From these data, the flow quality in the sub-channel is shown to be equivalent to that of other benchmark research facilities. Low Reynolds number experiments can be reliably performed using a sub-channel, as described, to modify the freestream flow.

4.2 Summary

A novel means of locally reducing the freestream velocity in open surface water channels has been devised and
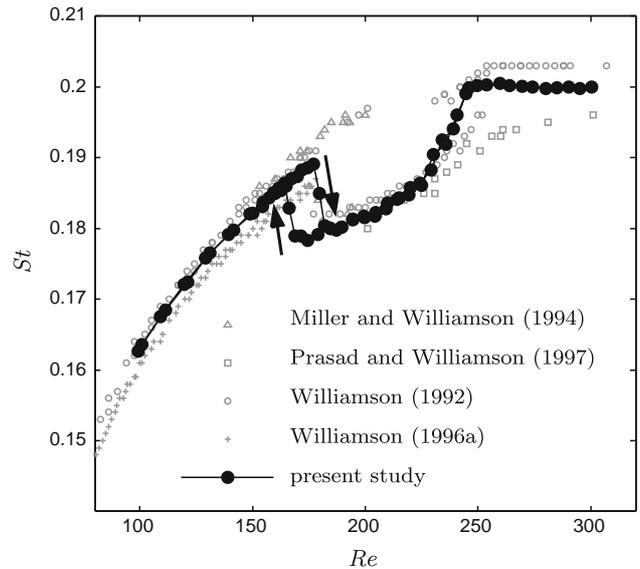
Fig. 9 Measurement of shedding frequency of a circular cylinder in the sub-channel (*filled circles*), in comparison to the literature data. The *arrows mark* the path through the hysteretic discontinuity when increasing (*arrow down*) and when decreasing (*arrow up*) the Reynolds number

demonstrated. It consists of a sub-channel insert with a perforated screen at its downstream end. The screen increases the pressure inside of this structure, leading to an uniform velocity reduction in the incoming flow. The porosity can be adjusted, meaning that the channel velocity can be reduced by 40–70 %. The rear two-thirds of the structure possess a constant streamwise velocity, with maximum variations below ± 2 % along the centreline.

To maintain adequate flow quality inside the sub-channel, following points must be considered:

1. The structure must be suspended above the main channel floor, leaving a gap of 5–10 mm. A rough estimate of the gap size is the displacement thickness of the main channel floor boundary layer.
2. Very low screen porosities, below $\alpha \approx 0.1$, should be avoided, as they lead to a strong deterioration of flow quality. The increased pressure gradient at low values of α results in large-scale flow separation on the bottom plate and beneath the free surface at the sub-channel entrance. A porosity above 0.15 is a good compromise between velocity reduction and flow quality.

The performance of the sub-channel has been demonstrated experimentally by recording the Strouhal–Reynolds number curve of a circular cylinder in cross-flow. All flow phenomena were reproduced, and the curve closely followed published data.

This investigation concludes that the flow velocity of an open surface water channel can conveniently be decreased

locally, by inserting a small channel section with a perforated screen at its downstream end. The flow quality is not diminished, provided certain conditions are met. This simple solution allows to perform low Reynolds number experiments in water channels that would otherwise not be capable of producing the required low flow velocities.

It should be noted that this initial version of a sub-channel can be further enhanced. In particular, the design of the intake can be optimised to improve profile uniformity, in conjunction with a gradient porosity of the screen. A slotted bottom plate might be effective in preventing boundary layer separation at very low velocities.

References

Bechert DW, Hoppe G, van der Hoeven JG, Makris R (1992) The berlin oil channel for drag reduction research. Exp Fluids 12(4–5):251–260

Carberry J, Sheridan J, Rockwell D (2005) Controlled oscillations of a cylinder: forces and wake modes. J Fluid Mech 538:31–69

Fouras A, Lo Jacono D, Hourigan K (2008) Target-free stereo PIV: a novel technique with inherent error estimation and improved accuracy. Exp Fluids 44(2):317–329

Leontini JS, Thompson MC (2012) Active control of flow-induced vibration from bluff-body wakes: the response of an elastically mounted cylinder to rotational forcing. In: 18th Australasian fluid mechanics conference. Launceston, Australia

Leontini JS, Lo Jacono D, Thompson MC (2011) A numerical study of an inline oscillating cylinder in a free stream. J Fluid Mech 688:551

Miller GD, Williamson CHK (1994) Control of three-dimensional phase dynamics in a cylinder wake. Exp Fluids 18(1):26–35

Nazarinia M, Lo Jacono D (2009) Flow behind a cylinder forced by a combination of oscillatory translational and rotational motions. Phys Fluids 21(5):051701-4

Nemes A, Zhao J, Lo Jacono D, Sheridan J (2012) The interaction between flow-induced vibration mechanisms of a square cylinder with varying angles of attack. J Fluid Mech 710:102–130

Prasad A, Williamson CHK (1997) Three-dimensional effects in turbulent bluff-body wakes. J Fluid Mech 343:235–265

Ryan K, Thompson MC, Hourigan K (2007) The effect of mass ratio and tether length on the flow around a tethered cylinder. J Fluid Mech 591:117–144

Vorobieff P, Ecke R (1999) Cylinder wakes in flowing soap films. Phys Rev E 60:2953–2956

Wang J, Birch J, Dickinson M (2004) Unsteady forces and flows in low reynolds number hovering flight: two-dimensional computations vs robotic wing experiments. J Exp Biol 207:449–460

Willert CE, Munson M, Gharib M (2010) Real-time particle image velocimetry for closed-loop flow control applications. In: 5th International symposium on applications of laser techniques to fluid mechanics. Lisbon

Williamson CHK (1992) The natural and forced formation of spot-like 'vortex dislocations' in the transition of a wake. J Fluid Mech 243:393–441

Williamson CHK (1996a) Three-dimensional wake transition. J Fluid Mech 328:345–407

Williamson CHK (1996b) Vortex dynamics in the cylinder wake. Annu Rev Fluid Mech 28(1):477–539